Resiliency-oriented Scheduling of Multi-microgrids in the Presence of Fuel cell-based Mobile Storage Using Hybrid Stochastic-Robust Optimization

ALIREZA AKBARI-DIBAVAR[1], KAZEM ZARE[1,*], SAJAD NAJAFI RAVADANEGH[2], AND VAHID VAHIDINASAB[3]

[1] *Faculty of Electrical and Computer Engineering, University of Tabriz, Tabriz, Iran*
[2] *Department of Electrical Engineering, Azarbaijan Shahid Madani University, Tabriz, Iran*
[3] *Department of Engineering, School of Science and Technology, Nottingham Trent University, NG11 8NS Nottingham, UK*
[*] *Corresponding author email: kazem.zare@tabrizu.ac.ir*

Manuscript received 04 February, 2024; revised 13 April, 2024; accepted 27 April, 2024. Paper no. JEMT-2402-1487.

In modern power grids, the hydrogen carrier contributes substantially. Hydrogen-based fuel cell vehicles also draw a path to a more sustainable society. This paper addresses the potential of hydrogen systems in a renewable-dominant multi-microgrid system to increase resiliency. The fuel cell-based trucks carry battery storage and act as emergency resources. A hybrid stochastic-robust optimization is proposed to optimize the scheduling plan for resources. The uncertainty of renewable output is handled by adjustable robust optimization whereas traffic of roads has been modeled using stochastic programming by using a dummy nodes and arcs model. A fuel management scheme is proposed to adjust the hydrogen fuel of the trucks. The results revealed that the corrective strategy, i.e., a combination of hydrogen facility and mobile storage improves the overall resiliency indexes. In this regard, the area covered under the resiliency trapezoid increased up to 90% under the robust case. The critical load curtailment decreased from 38.65 MW to 30.08 MW under the risk-neutral case and from 50.78 MW to 42.17 MW under the risk-averse case. The system is stronger with the proposed corrective strategies and the ramp of resiliency fall has been decreased from 0.285 to 0.199 and from 0.382 to 0.293 under risk-neutral and risk-averse cases, respectively. Finally, the replacement of a hydrogen storage system with a stationary battery storage system revealed that the stationary battery storage similarly reduces the load curtailment however the presence of hydrogen storage helps the MBS refueling which directly influences the load recovery performance.

keywords: *Multi-microgrid, Hydrogen facility, Mobile energy storage, Stochastic programming, Robust optimization approach.*

http://dx.doi.org/10.22109/JEMT.2024.441626.1487

NOMENCLATURE

t Index of time
s Index of scenario
m, n Index of microgrid
α, β Index of real station for MBS units
tr Index of MBS unit
Ω^{st} Set of real stations
(m, a) Conjunction points of a microgrid and a real station for the MBS unit

Parameters

π_h^{elec} Hourly electricity price ($/MW)
α_i The grid outage indicator equals zero whenever the grid is available
$Voll^{CL}$,$Voll^{NCL}$ Value of lost critical and non-critical loads ($/MW)
$P_{t,m}^{CL}$ Electrical critical load demand of microgrid m in the period t (MW)
$P_{t,m}^{NCL}$ Electrical non-critical load demand of microgrid m in

period t (MW)

$P_{m,n}$ Maximum exchangeable power between microgrids m, n (MW)

$\overline{P_{tr}^{mbs}}$ Maximum charging/discharging power capacity of MBS units (MW)

η_{tr}^{mbs} The MBS power charging and discharging efficiency (%)

$\underline{EC_{tr}^{mbs}}$, $\overline{EC_{tr}^{mbs}}$ Minimum and maximum electric storage capacity of MBS unit (MWh)

EC_0^{mbs} Initial state of electric energy of MBS unit (MWh)

$P_{t,m}^{W}$ Forecasted wind power of wind turbines in microgrid m in the period (MW)

$P_{t,m}^{PV}$ Forecasted solar power of photovoltaic panels in microgrid m in the period t (MW)

$\underline{T_{tr}^{H2}}$,$\overline{T_{tr}^{H2}}$ Minimum and maximum fuel capacity of MBS unit (kg)

W_m^0 Initial available hydrogen gas in the tank of microgrid m (kg)

$\underline{W_m^{H2}}$,$\overline{W}_m^{H2}$ Minimum and maximum capacity of hydrogen tank of microgrid m (kg)

C^{H2} The fuel consumption coefficient of MBS unit (kg/km)

P_t^{Grid} Purchased power from the main grid in the period (MW)

$[PC_{t,s,m}^{mbs}$, $PD_{t,s,m}^{mbs}$ Charged and discharged powers of the MBS unit attached to the microgrid m in the period t and scenario s (MW)

$P_{t,s,m,n}$ Power is exchanged between microgrids when connected to the PCC in the period $t$and scenario s (MW)

$Lsh_{t,s,m}^{CL}$ Amount of critical load curtailment of microgrid m in the period t and scenario s (MW)

$Lsh_{t,s,m}^{NCL}$ Amount of non-critical load curtailment of microgrid m in the period t and scenario s (MW)

$P_{t,s}^{P2H}$ Consumed power to convert electric energy into hydrogen gas in the period t and scenario s (MW)

$P_{t,s}^{H2P}$ Produced power by the fuel cell device in the period t and scenario s (MW)

$W_{t,s,m}^{H2}$ The hydrogen stored in the tank of microgrid m in the period t and scenario s (kg)

$H_{t,s,m}^{WE}$ The hydrogen gas produced by the water electrolyzer in the period t and scenario s (kg)

$H_{t,s,m}^{FC}$ The hydrogen gas deployed by fuel cell device to regenerate electric power in the period t and scenario s (kg)

$H_{t,s,tr}^{RF}$ The hydrogen gas consumed for refueling the MBS unit tr in the period t and scenario s (kg)

$H_{t,s,tr}^{travel}$ The hydrogen gas consumed for traveling the MBS unit tr in the period t and scenario s (kg)

$EC_{t,s,tr}^{mbs}$ Electrical energy stored by MBS units in the period t and scenario s (MWh)

$uc_{t,s,m,tr}^{mbs}$, $ud_{t,s,m,tr}^{mbs}$ Binary variables indicating the charging and discharging status of the MBS unit attached to the microgrid m in the period t and scenario s

$T_{t,s,tr}^{H2}$ The hydrogen fuel stored in the tank of the MBS unit in the period t and scenario s (kg)

$I_{\alpha,\beta,t,s,tr}$ Binary variable equals 1 when the truck tr traveling path in the period t and scenario s

Abbreviations

ESS Electric energy storage

FC Fuel cell

$GAMS$ General algebraic modeling system

MBS Mobile battery storage

MDG Mobile diesel generator

PV Photovoltaic

WE Water electrolyzer

1. INTRODUCTION

The large-scale power outages caused by natural disasters can cause a vast socio-economic loss nowadays due to an intensive dependence on electric energy. The main challenge for the system operator is to serve critical loads such as communication, healthcare, and sensitive industries aftermath of the drastic events. The continued power outage after the natural events also exaggerates the disasters such as reduced emergency activities for survival. The ability of the power system to resist, absorb, and respond to such a huge event is studied in the field of resiliency. A resilient energy system can withstand fatal damages, recover to a stable operation as soon as possible, and restore a large portion of loads. Evidently, conservative investments in the system enhance resiliency. The use of distributed generation, undergrounding the electric infrastructures, formation of microgrids and sharing data, investment in flexibility, automation, and communication technologies. all are introduced as hardening alternatives for grid resilience enhancement [1,2]. The hardening strategies are pre-event activities. On the other hand, operational strategies respond to the consequences of massive disasters. The optimal spinning reserve deployment, reconfiguration of the grid topology and coordination of power-gas networks, dispatch of repair crews, and use of the mobile emergency generators, and energy storage devices are prominent post-event solutions that could be included with different preventive scheduling frameworks [3,4]. Hydrogen is considered a carrier that can be stored on a long-term and large scale that can help the grid operation and efficiency [5]. The integration of flexible resources such as hydrogen storage is investigated as a probable alternative to increase the power grid resilience [6]. The authors of [7] have assessed the effectiveness of the hydrogen carrier in the microgrids' resilient operation and found out the critical role of the hydrogen systems in supporting islanded microgrids. The hydrogen carrier is also prescribed in [8] as a sustainable solution to enhance the resilience of integrated hydrogen-power-heat microgrids. The authors emphasized the synergic operation of various energy resources and concluded that the integration of hydrogen carriers can remarkably help in the load restoration process. On the other hand, the realization of the renewable-dominant grids invokes a large-scale installation and deployment of EES. Among the available ESS technologies, electrochemical battery storage systems are popular due to higher operation efficiency, modular construction, adjustable power and energy rates, and movability. This is becoming a reason for implementing battery storage systems for resiliency-oriented studies [9]. The use of movable battery storage (MBS) has been addressed to increase the efficiency and resiliency of the power grids. In this concept, the battery storage devices with grid interconnecting facilities are mounted on vehicles to move in a Spatiotemporal network. The MBS units are commonly self-powered or diesel-based to move and can deliver active and

reactive power services to the networks. The main advantage of MBS compared with a stationary battery storage system is the increased flexibility whereas the system operator can change the location of the energy storage services [10]. Hence, the MBS can play the role of a stationary storage system under normal operation and can be used for load restoration in the aftermath of disasters. The MBS unit is a proper solution to electrify the damaged parts of the power grid where the electric connection has been lost due to generation outages or fallen lines. In this regard, the load restoration process can be accomplished if there is a way to recharge the MBS [11]. In recent years, MBS units with massive energy capacity for utility applications have been offered commercially [12]. There are several works that address the MBS unit's proactive pre-positioning and allocation in the power system to enhance load supply resiliency. Chen et al. [13] addressed the problem of the reliability assessment of the integrated power distribution grids with MBS systems and proved the enhanced performance. Their evaluation revealed that the expected energy not supplied is positively correlated with the capacity of MBS units. However, the spatial and temporal model for the transportation network is missed, and the effect of the road traffic is modeled as a time delay for deployment of the MBS units. The authors of [14] proposed a two-stage optimization framework to optimize the investment on the MBS units at the first stage and re-route the installed MBS units at the second stage to reduce the load shedding amount and form microgrids according to the circumstances. Ref. [15] proposed an optimization algorithm to coordinate the bidding process of the microgrids in the day-ahead and real-time markets and eventually allocate the MBS units. By conducting a two-stage optimization, the authors have evaluated the self-healing index improvement of the grid resiliency due to the allocated MBS units. In [16], the potential of battery electric buses has been assessed in the microgrid resiliency during islanded operation. In this context, the battery electric buses serve as flexible resources to help renewable power output smoothness and supply the critical loads, and also serve as backup resources for black startup programs. In [17], the resiliency of urban integrated power and gas networks has been studied against destructive rainstorms. In this manner, a multi-stage optimization problem is designed to first make decisions regarding the hardening strategies and dispatch the resources and repair crews after the worst-case event considering the real-time traffic of paths. In [18], the stationary and MBS units are nominated as corrective options for increasing the resiliency of the microgrids and the authors tend to optimize the size, location, and routs of the ESS and MBS units to maximize the restored loads. Ref. [19] takes into account the stochasticity nature of renewable generation while trying to enhance the resiliency grid with the help of MBS units. In other words, using a probabilistic approach, the electric loads restoration process has been accomplished by optimal routing and scheduling of MBS units. The application of a mobile diesel generator (MDG) beside the MBS units for increasing the resiliency in an integrated power and gas system is prescribed in [20] to serve the electric and heat loads during outages. The movability time scales of the MBS and diesel generators are assumed hourly and seasonally, respectively. Moreover, using a probabilistic method the uncertainties of the renewable generation and loads are incorporated. Recently, in [21] a stochastic programming framework has been designed to enhance the resiliency of electric load supply for an integrated power and gas network where the MBS units are dispatched to serve loads after transmission lines' outage. However, the spatiotemporal constraints, uncertainties of renewables, and traffic times have not been considered. With a sophisticated integration between the power and transportation networks, traffic network modeling and its importance are magnified in recent studies. The static traffic network models are suitable for long-term planning problems [22], whereas, for the resiliency case, the short-term load restoration with updated traffic information is of great importance. In this regard, the authors of [23] presented coordinated corrective services including an energy resource scheduling plan, MBS unit dispatch, and network reconfiguration to enhance the resiliency of a power distribution network. Their proposed method is based on a rolling horizon with updated information about the electric and transportation networks corridors and their associated uncertainty as well as load stochasticity are modeled using scenario-based stochastic technique. The authors of [24] addressed the problem of optimal dispatch problem of MDG, MBS units, and repair crews by emphasizing the impacts of traffic time caused by rad congestion aftermath of the disasters. The authors defined a weighted dynamic traffic assignment problem and cell transmission model to minimize the travel times of the resources and maximize the restored critical loads in a sample power grid. Analogously, the dispatch problem of the MDG, MBS units, and repair crews has been studied in [25], and the influence of each restoration strategy is evaluated in a power grid case study. Finally, the role of the MBS units in grid resilience improvement is assessed by [26] using a rolling-horizon optimization problem that considers different outage scenarios and the congestion of roads that is modeled by doubling the travel time and cost.

A. Contributions

The field of power grid resiliency has been studied in recent years with different perspectives and methodologies. The common objectives of the studies were the critical loads restoration very quickly and with an efficient strategy. The MBS units were proposed as one of the great opportunities for load restoration. The previous studies are well structured and fill the main gaps. However, a transition towards renewable-dominant microgrids faces intermittent power output challenges the resiliency-oriented scheduling problems. The destructive effects of uncertainties are remarkable during the faulty conditions and it is needed to take serious actions to serve the loads. The uncertainties in renewable generation and the traffic flow of the roads for the MBS units have been studied in this paper using a hybrid stochastic-robust approach that has not been addressed due to the authors' knowledge. Moreover, the MBS units are not always self-powered, and considering travel costs cannot provide a technical sight. In reality, the operation of the MBS units is restricted to the traffic state and corresponding fuel consumption which has not been addressed in the recent studies. For a detailed comparison among the mentioned studies to reveal the net contributions, Table 1 presents the related works in the field of resiliency with mobile emergency resources. From Table 1, the four main contributions of this paper are listed as follows.

- Proposing a hybrid two-stage stochastic-robust approach for resilient operation of fully renewable multi-microgrids with MBS units. This approach makes the system operator able to handle the severe renewable uncertainties based on the traffic flow scenarios

- Proposing an integrated operation of power and hydrogen systems, including water electrolyzer, hydrogen storage, and fuel cell to improve the flexibility and maximize the

load restoration in coordination with the MBS units routing schedule.

- Proposing a dynamic fuel management model for the studied hydrogen-based trucks to facilitate the security of the critical load restoration process.

- Establishing A.L.R.T. resiliency assessment index to evaluate the performance of the proposed scheme

B. Paper organization

The rest of the paper is organized as follows. The problem modeling including the integrated power-hydrogen-transportation multi-microgrid system is presented in section 2. Section 3 presents the testbed schematic and required information for the simulation. Moreover, the results are presented and discussed in section 3. The paper is concluded and main findings are discussed in section 4 as the conclusion.

2. PROBLEM MODEL

As mentioned, the resiliency-oriented problem in this paper is dedicated to a fully renewable multi-microgrid system integrated with the urban transportation system and hydrogen facility. To develop a comprehensive framework that can be used in real cases, the coordinated resource management and the MBS routing are considered corrective actions after extreme events. To effectively involve the uncertain behavior of renewable resources and the traffic state of the connective roads, a hybrid stochastic-robust approach is proposed to take the advantages of both approaches [27]. Stochastic programming with discrete scenarios is beneficial for modeling the uncertainty of state of the road traffic, whereas the robust optimization with an adjustable budget of uncertainty is useful for modeling severely uncertain parameters, such as wind and solar power generation. To this end, for any budget of uncertainty, the resilient scheduling of the multi-microgrid has been accomplished by solving a stochastic programming, and minimizing the expected cost at each step. A schematic of the proposed uncertainty-aware scheduling method is depicted in Fig. 1 [33].

The concept of vehicle routing problem with the proposed stochastic programming for traffic status lets the system operator choose the best routing scheme for the MBS units subject to road congestion and available fuel in their tank. To consider the traffic effects of the paths, the dummy nodes and arcs model is proposed in this paper which could be integrated with the transportation network with mixed-integer linear formulation. In this model, the path between two real stations is divided by several virtual stations with the same time span. This assumption can effectively model the time delays for travel and also the fuel consumption of the MBSs that have been stuck in a traffic jam. As an example, Fig. 2 shows a path between two stations (i.e., microgrid), in which the traffic flow of the path could be modeled through a virtual station.

A. Mathematical formulation

The main objective is to minimize the operational cost while after the main power grid outage, the main objective is to elevate the critical load of the microgrids. The objective function is defined

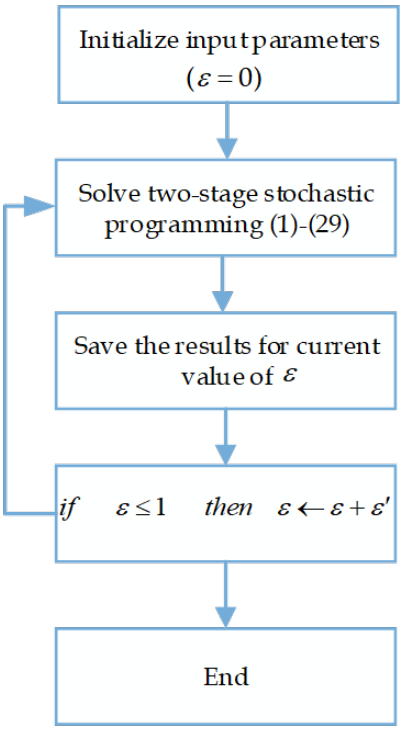

Fig. 1. The flowchart of the proposed hybrid stochastic-robust approach [33]

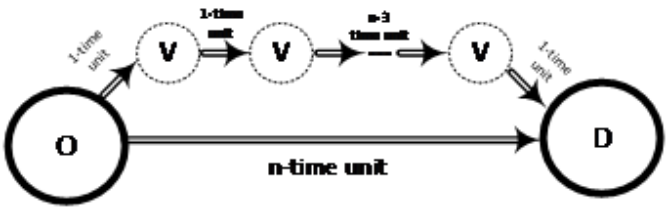

Fig. 2. The concept of dummy arcs and nodes to model the traffic jam

Table 1. A detailed comparison between recent published works with their pros and cons

Ref	Transportation model	Uncertainty renewable and load	Traffic on the path	Fuel management	Fully renewable	Resiliency strategy
[13]	×	×	✓	×	×	MBS
[14]	✓	×	×	×	×	MBS
[15]	×	✓	×	×	×	MBS
[16]	✓	×	×	×	×	$Electricbuses$
[17]	✓	×	✓	×	×	RC
[18]	×	×	×	×	×	$ESS-MBS$
[19]	✓	✓	×	×	×	MBS
[20]	×	✓	×	×	×	$MBS-MDG$
[21]	×	×	×	×	×	$MBS-RC$
[23]	✓	✓	✓	×	×	MBS
[24]	✓	×	✓	×	×	$MBS-MDG-RC$
[25]	✓	×	✓	×	×	$MBS-MDG-RC$
[26]	✓	×	✓	×	×	MBS
This Paper	✓	✓	✓	✓	✓	$MBS-hydrogensystems$

as (1).

$$\min \sum_t P_t^{Grid} \times \pi_t^{elec} + \sum_{t,s,m} \lambda_s \times (Lsh_{t,s,m}^{CL} \times Voll^{CL} + Lsh_{t,s,m}^{NCL} \times Voll^{NCL}) + \sum_{t,s,m} \lambda_s \times (H_{t,s,m}^{WE} \times \pi^{WE}) \quad \textbf{(1)}$$

The objective function in (1) minimizes three items, respectively, the cost of electric power exchange with the main grid, and the load curtailment penalty that is different for critical and non-critical loads and the cost of hydrogen production. Taking into account that the objective function tries to optimize the expected cost considering the probability of scenarios of congested roads. It is notable that the power exchange with the utility grid is not dependent on the scenario and should be treated as a here-and-now decision variable. As the main objective is to serve active loads during contingencies, the power flow equations are simplified to the active power balance in (2) and security limits in (3)-(5). Equations (6)-(11) represent the operation of the MBS units and associated limits. It should be noted that the charging and discharging processes happen at the station in each microgrid.

$$P_{t,s}^{Grid} + P_{t,s}^{H2P} - P_{t,s}^{P2H} + P_{t,m}^{W} + P_{t,m}^{PV} + (Lsh_{t,s,m}^{CL} - P_{t,s,m}^{CL}) + (Lsh_{t,s,m}^{NCL} - P_{t,s,m}^{NCL}) + \sum_{tr}(PD_{t,s,m}^{mbs} - PC_{t,s,m}^{mbs}) = \sum_n P_{t,s,m,n} \quad \forall t,s,m \quad \textbf{(2)}$$

$$-(1-\alpha_t) \times \overline{P_{m,n}} \leq P_{t,s,m,n} \leq (1-\alpha_t) \times \overline{P_{m,n}} \forall t,s,m,n \quad \textbf{(3)}$$

$$0 \leq Lsh_{t,s,m}^{CL} \leq P_{t,s,m}^{CL} \quad \forall t,s,m \quad \textbf{(4)}$$

$$0 \leq Lsh_{t,s,m}^{NCL} \leq P_{t,s,m}^{NCL} \quad \forall t,s,m \quad \textbf{(5)}$$

$$0 \leq PC_{t,s,m,tr}^{mbs} \leq uc_{t,s,m,tr}^{mbs} \times \overline{P_{tr}^{mbs}} \quad \forall t,s,tr,m \in \Omega^{st} \quad \textbf{(6)}$$

$$0 \leq PD_{t,s,m,tr}^{mbs} \leq ud_{t,s,m,tr}^{mbs} \times \overline{P_{tr}^{mbs}} \quad \forall t,s,tr,m \in \Omega^{st} \quad \textbf{(7)}$$

$$uc_{t,s,m,tr}^{mbs} + ud_{t,s,m,tr}^{mbs} \leq 1 \quad \forall t,s,tr,m \in \Omega^{st} \quad \textbf{(8)}$$

$$EC_{t,s,tr}^{mbs} = EC_{t-1,s,r}^{mbs} + \sum_m \eta_{tr}^{mbs} PC_{t,s,m}^{mbs} - PD_{t,s,m}^{mbs}/\eta_{tr}^{mbs} \quad \forall t,s,m,tr \quad \textbf{(9)}$$

$$\underline{EC_{tr}^{mbs}} \leq EC_{t,s,tr}^{mbs} \leq \overline{EC_{tr}^{mbs}} \quad \forall t,s,tr \quad \textbf{(10)}$$

$$EC_{t,s,tr}^{mbs} = EC_0^{mbs} \quad \forall t = 1, t = 24, s, tr \quad \textbf{(11)}$$

The hydrogen energy system integrated with the power microgrids enhances the flexibility of operation and provides a short-time energy storage capability. Moreover, it provides the required fuel for the trucks to travel and accomplish the load restoration process. The feasibility constraints for the hydrogen operation have been presented in (12)-(15) according to [28]. Constraints (12) and (13) model the operation of water electrolyzer and fuel cell devices, respectively. The electric power consumed in Equation (12) is used to produce a certain amount of hydrogen gas based on the water electrolyzer coefficients. Similarly, a certain amount of hydrogen gas is deployed by the fuel cell to regenerate the electric power (13). The operation of the hydrogen system is completed with a hydrogen tank, where its dynamics are shown in (14) and the related limits in (15).

$$H_{t,s,m}^{WE} = \frac{P_{t,s,m}^{P2H}}{\varphi^{WE}} \eta^{WE} \quad \forall t,s,m \quad \textbf{(12)}$$

$$P_{t,s,m}^{H2P} = H_{t,s,m}^{FC} \varphi^{FC} \eta^{FC} \quad \forall t,s,m \quad \textbf{(13)}$$

$$W_{t,s,m}^{H2} = W_m^0 + H_{t,s,m}^{WE} - H_{t,s,m}^{FC} - H_{t,s,m}^{RF} \quad \forall t,s,m \quad \textbf{(14)}$$

$$\underline{W_m^{H2}} \leq W_{t,s,m}^{H2} \leq \overline{W}_m^{H2} \quad \forall t,s,m \quad \textbf{(15)}$$

The transportation system model in (16)-(20) known as the vehicle routing problem (VRP) represents the spatial-temporal equations that the feasible routing for the MBS is restricted. The location of each MBS unit in the network is identified by a binary variable that shows the travel on the roads and immobility at the stations. Equation (16) shows that at every time slot, each traveling vehicle should be in one position exclusively. Equation (17) models the traveling states and updates the location of each MBS. Equations (18) and (19) identify the initial and final locations of the MBS units in the network at the beginning and end of scheduling with the help of binary indicators and . Finally, the charging and discharging ability for the MBS units is activated only if the MBS remains in a real station in one of the microgrids. This fact has been modeled in (20) by defining the binary variable which equals 1 only if the origin and destination nodes are the same.

$$\sum_{(\alpha,\beta)} I_{\alpha,\beta,t,s,tr} = 1 \quad \forall(\alpha,\beta),t,s,tr \tag{16}$$

$$\sum_{(\alpha,\beta)} I_{\alpha,\beta,t,s,tr} = \sum_{(\alpha,\beta)} I_{\beta,\alpha,t+1,s,tr} \quad \forall(\alpha,\beta),t,s,tr \tag{17}$$

$$\sum_{(\alpha,\beta)} I_{\alpha,\beta,t,s,tr} = \mathrm{I}_{tr}^{ini} \quad \forall(\alpha,\beta),t=1,s,tr \tag{18}$$

$$\sum_{(\alpha,\beta)} I_{\alpha,\beta,t,s,tr} = \mathrm{I}_{tr}^{fin} \quad \forall(\alpha,\beta),t=24,s,tr \tag{19}$$

$$uc_{t,s,m,tr}^{mbs} + ud_{t,s,m,tr}^{mbs} \leq \mathrm{X}_{\alpha,\alpha,t,s,tr} \quad \forall t,s,tr,(m,a) \tag{20}$$

This paper proposes a model to manage the capacity of vehicle tanks for emergency tasks in (21)-(24). The trucks in this paper are refueled in the hydrogen stations. For mobility, each MBS should schedule the refueling plan according to the state of traffic and the travel signal. It is assumed that the hydrogen refueling stations are established within the microgrids with hydrogen infrastructures. Equation (21) calculates the hydrogen consumption of the MBS during each trip. It is assumed that the traffic congestion will increase fuel consumption by 50% compared with normal conditions. Equation (22) models the dynamics of the fuel tank of MBS units. Based on equation (23), the refueling process will be done when the MBS reaches and attaches to a real refueling station. Finally, equation (24) shows the capacity limits of the fuel tank.

$$H_{t,s,tr}^{travel} = C^{H2} \times \sum_{(\alpha\neq\beta)} I_{\alpha,\beta,t,s,tr} \quad \forall t,s,(\alpha,\beta),tr \tag{21}$$

$$T_{t,s,tr}^{H2} = T_{t-1,s,tr}^{H2} + H_{t,s,tr}^{RF} - H_{t,s,tr}^{travel} \quad \forall t,s,tr \tag{22}$$

$$0 \leq H_{t,s,tr}^{RF} \leq \overline{H_{tr}^{RF}} \times \mathrm{X}_{\alpha,\alpha,t,s,tr} \quad \forall t,s,tr \tag{23}$$

$$\underline{T_{tr}^{H2}} \leq T_{t,s,tr}^{H2} \leq \overline{T_{tr}^{H2}} \quad \forall t,s,tr \tag{24}$$

Till here, the resiliency-oriented scheduling problem (1)-(24) tries to recover the load after an extreme event that led to tie-lines outage by using as a risk-neutral problem considering the effects of road congestion using stochastic programming. However, due to a strong reliance on renewable generation, the resiliency of the system is associated with considerable risk. The renewable forecast error can impose huge power deficiency during grid outages. The robust optimization approach has been widely used for modeling the uncertainty behaviors in energy systems. The initial formulation for the robust optimization problem forms a min-max optimization problem and should be recast into single-level problems using complementarity constraints and strong duality theorem that leads to the introduction of several auxiliary variables and constraints known as robust counterparts. The robust counterparts can be used in this paper to integrate the uncertainties of the renewable generation as follows.

$$\begin{aligned} &P_{t,s}^{Grid} + P_{t,s}^{H2P} - P_{t,s}^{P2H} + (P_{t,m}^{W} - \psi^1\varepsilon - x_{t,s,m}^1) + \\ &(P_{t,m}^{PV} - \psi^2\varepsilon - x_{t,s,m}^2) + (Lsh_{t,s,m}^{CL} - P_{t,s,m}^{CL}) + (Lsh_{t,s,m}^{NCL} - P_{t,s,m}^{NCL}) \\ &+ \sum_{tr}(PD_{t,s,m}^{mbs} - PC_{t,s,m}^{mbs}) = \sum_{n} P_{t,s,m,n} \quad \forall t,s,m \end{aligned} \tag{25}$$

$$\begin{aligned} \psi^1 + x_{t,s,m}^1 &\geq (\overline{P_{t,m}^{W}} - \underline{P_{t,m}^{W}}) \times z_{t,s,m}^1 \\ \psi^2 + x_{t,s,m}^2 &\geq (\overline{P_{t,m}^{PV}} - \underline{P_{t,m}^{PV}}) \times z_{t,s,m}^2 \end{aligned} \tag{26}$$

$$\begin{aligned} z_{t,s,m}^1 &\geq 1 \\ z_{t,s,m}^2 &\geq 1 \end{aligned} \tag{27}$$

$$x_{t,s,m}^1, x_{t,s,m}^2 \geq 0 \tag{28}$$

$$\psi^1, \psi^2 \geq 0 \tag{29}$$

By considering the uncertainty effects using the adjustable robust optimization approach, the power balance equation is changed according to (25), which is the robust control parameter. Equations (26)-(29) represent the robust counterparts, in which ψ , ,$x_{t,s,m}$ and $z_{t,s,m}$ are positive continuous auxiliary variables that have been created during the recasting of the original robust optimization problem [29].

3. NUMERICAL EVALUATIONS

This section describes the details of the case study, input data, and constants, the numerical results for the resource schedule, and resiliency improvement analysis.

A. The case study

A schematic of the studied multi-microgrid system is shown in Fig. 3. The testbed consists of six microgrids with full renewable generation, and MBS units on the roads. The contiguous microgrids have a common road for commuting. Detailed information about microgrids is presented in Table 2 has been taken from [30] with some modification in the rated capacity of wind and solar resources and the loading is adopted by the generation capacity. The total load of each microgrid is divided into controllable (non-critical) and critical loads based on the shares provided in the reference. Microgrids 2 and 4 are equipped with hydrogen generation, storage, and fuel cell technology that enhances the overall flexibility and are the main targets for the MBS units for refueling. To model the resilient operation, it is assumed that a drastic event leads to a power grid outage between 10:00 to 17:00 (peak load time).

The energy conversion coefficients as well as other required constants are presented in Table 3. Table 4 represents the hourly electricity price in which the microgrids trade electricity with the utility. Note that Table 2 represents the rated power consumption and generation while for a multi-time scheduling plan, the time factors should be provided. Figure 4 shows the hourly time factors for the load consumption, renewable generation, and corresponding confidence intervals. For clearness, the forecasted values for the wind and solar generation are subjected to ±20% and ±10% errors, respectively, considering their volatile nature. Moreover, the information on the congested road scenarios is presented in Table 5. It is assumed that the congestion of roads

Table 2. Detailed information about microgrid characteristics

Microgrid No.	Peak non-critical load (MW)	Peak critical load (MW)	Rated capacity of wind turbines (MW)	Rated power of PV panels (MW)	Hydrogen storage capacity (kg)	Hydrogen refueling station
m=1	1	4	2	1.5	0	×
m=2	1.5	1	1	1	100	✓
m=3	1	2.5	1	0.5	0	×
m=4	1	3	3	0	100	✓
m=5	1.5	5.5	2	1	0	×
m=6	1	1.5	1	1	0	×

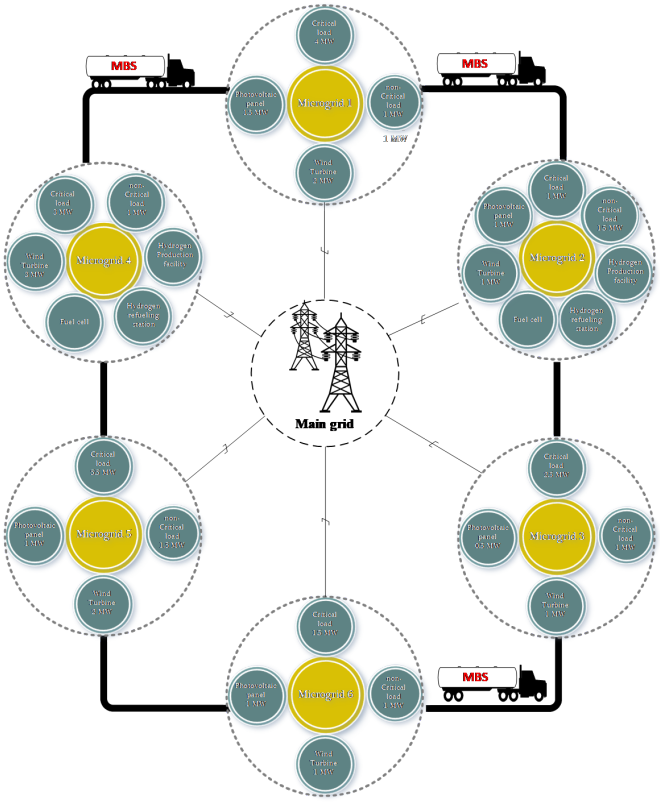

Fig. 3. The design of the studied multi-microgrids with connective roads

Table 3. The constants and conversion coefficients

Character	Value	Character	Value
$Voll^{NCL}$,$Voll^{CL}$	100 \$/MW, 200 \$/MW	η^{WE}	80%
EC_0^{mbs}	0.25 MWh	φ^{WE}, φ^{FC}	0.04 MW/kg
$\underline{EC_{tr}^{mbs}}$, $\overline{EC_{tr}^{mbs}}$	0.25 MWh, 2 MWh	C^{H2}	1 kg per 100 km
$\overline{P_{tr}^{mbs}}$	1 MW	$\underline{T_{tr}^{H2}}$,$\overline{T_{tr}^{H2}}$	0 kg, 50 kg
η_{tr}^{mbs}	90%	$\sum_{(\alpha,\beta)} I_{t,s,\alpha,\beta}$	100 km
$\underline{W}_m^{H2}$, $\overline{W}_m^{H2}$	0, 100 kg		

happens in the rush times, between 8:00 to 13:00 and 18:00 to 20:00 in all scenarios, and expands the travel time by double. For example, scenario 1 represents the case without congested roads, where the travel on the roads takes 1 hour, while under scenario 2, the travel between microgrids 1 and 2 takes 2 hours for instance.

B. Simulation results

The proposed method has been modeled as mixed-integer linear programming (MILP) in the GAMS optimization package and solved using the CPLEX solver [31]. For a case in which the main grid is out of service, the simulation has been carried out. However, without loss of generality, the proposed scheme can be applied to other contingency cases. With this respect, the scheduling plan for the resources has been found for every operational scenario, as the MBS unit dispatch is scenario-based. To focus on the role of the MBS units, the scheduling plans are shown for scenario 12, where the paths $1 \leftrightarrow 4$ and $3 \leftrightarrow 6$ are simultaneously congested in the rush time. It should be noted that all of the microgrids are connected to the grid through PCC, and aftermath of the grid outage they will be separated due to stability issues. Figure 5 shows the total exchanged power between the main grid and the whole multi-microgrid system under both risk-neutral and risk-averse strategies. It should be noted that the risk-averse decision-maker anticipates the worst realization of the renewable output by setting . This anticipation results in conservative power contracts with the utility grid with a higher level of power purchasing, especially after the fault due to the loss of solar generation capacity. From Fig. 5,

Table 4. The hourly wholesale electricity price of the main grid

Price ($/MW)	Time (hour)
70	1
65	2
60	3
58	4
59	5
63	6
70	7
77	8
75	9
70	10
63	11
57	12
55	13
57	14
63	15
67	16
70	17
73	18
71	19
64	20
56	21
52	22
50	23
48	24

Table 5. The congested road scenarios

	1-2	1-4	2-3	4-5	5-6	3-6
Scen.1	×	×	×	×	×	×
Scen.2	✓	×	×	×	×	×
Scen.3	×	✓	×	×	×	×
Scen.4	×	×	✓	×	×	×
Scen.5	×	×	×	✓	×	×
Scen.6	×	×	×	×	✓	×
Scen.7	×	×	×	×	×	✓
Scen.8	✓	×	×	×	×	✓
Scen.9	✓	×	×	×	✓	×
Scen.10	✓	×	×	✓	×	×
Scen.11	×	✓	✓	×	×	×
Scen.12	×	✓	×	×	×	✓
Scen.13	×	✓	×	×	✓	×
Scen.14	×	×	✓	✓	×	×
Scen.15	×	×	×	✓	×	✓
Scen.16	×	×	✓	×	✓	×

Fig. 4. The time factor constants for the load consumption and renewable generation

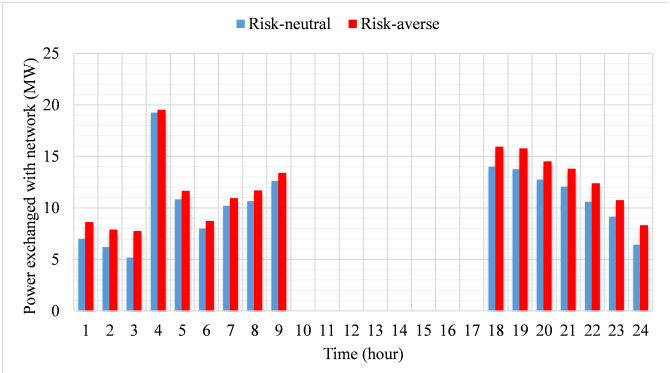

Fig. 5. The total exchanged power with the main grid

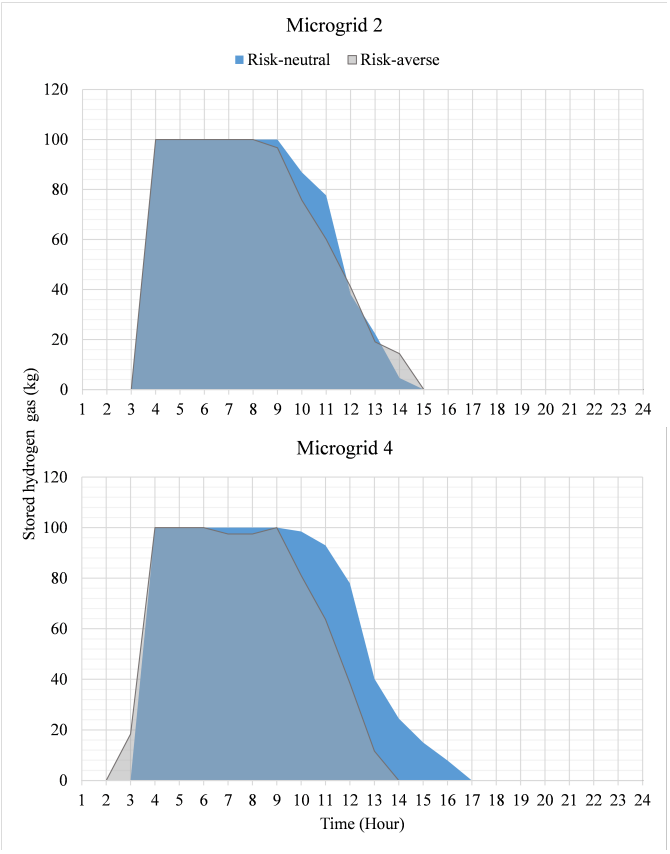

Fig. 6. The volume of hydrogen stored in the hydrogen tanks

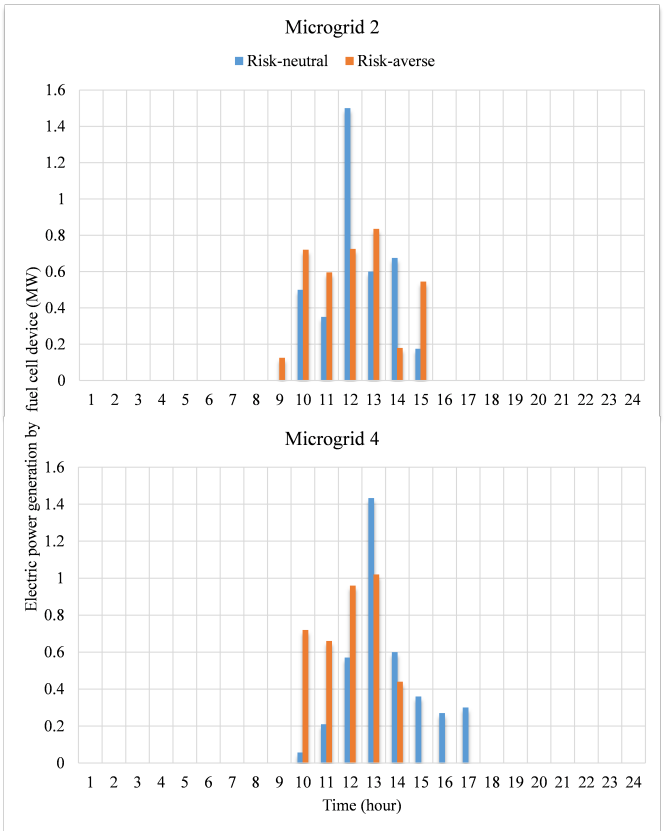

Fig. 7. The electrical power generated by the fuel cell device

the grid is unavailable from hour 10:00 to 17:00 and the evaluation of resiliency in these hours reveals the effectiveness of the proposed risk-based scheduling framework. The traded power with the power grid is not dependent on the scenarios and the system manager makes contracts with the utility in the day-ahead market. During normal operation, due to the connection of multi-microgrids and shared renewable generation, the total purchasing power is lower than the actual demand for microgrids. The integration of hydrogen systems enhances flexibility and can be considered a proactive strategy for resiliency enhancement. Both risk-neutral and risk-averse decision-makers will take advantage of the hydrogen system to recover the loads after grid outage. This includes producing hydrogen during off-peak times with cheaper electricity through water electrolysis and storing the hydrogen gas in the tank. Figure 6 shows the dynamics of the hydrogen tanks in microgrids 2 and 4. Both hydrogen tanks are filled at hour 4:00 a.m. to be reused by the fuel cell device during outage times to generate electric power and to refuel the MBS units to accomplish the load restoration task. The results indicate that the system manager produces about 200 kg of hydrogen under both risk-neutral and risk-averse cases and the involvement of water electrolyzer cost could not change the overall scheduling since the value of load restoration is more influencing in resiliency-oriented operation. To reveal the differences between risk-neutral and risk-averse strategies in deploying the stored hydrogen, the power generation scheduling for the fuel cell devices is shown in Fig. 7. By matching Figures 6 and 7 it can be concluded that the dynamics of the hydrogen tank exactly follows the demand of fuel cell device. The hydrogen demand of trucks is also provided by the hydrogen tank directly slightly changes the volume of the hydrogen tank in Fig. 6. From Fig. 7, the fuel cell device is mainly used during the outage times. Since there is no electrical connection between microgrids during the outage time, the power generation of the fuel cell is limited to the local power demand. The investigation shows that the cumulative power generation by the fuel cell is about 3.8 MW under both risk-neutral and risk-averse cases due to the limited capacity of hydrogen storage. However, the differences come from different resource scheduling. For instance, at hours 12:00 and 13:00 under the risk-neutral case, the generated power of the fuel cell goes up remarkably due to the presence of the MBS units in the corresponding microgrid. Moreover, a conservative perspective regarding renewable generation implies a non-critical load curtailment under the risk-averse case. Hence, the generated power by the fuel cell is not enough to cover both critical and non-critical loads at hour 14:00 in microgrid 2. Instead, the capacity of the hydrogen storage is used to recover the critical loads at the future time slots. The main cost of the fuel cell operation is related to the procurement of hydrogen cylinders. In the studied case, the microgrids are equipped with hydrogen production (i.e., water electrolyzer) and storage facility that reduces the operating cost of the fuel cell systems. Moreover, as the fuel cell is used as a backup resource to recover the curtailed loads, it is economical to install and use this technology to provide electric power. The involvement of the operating cost of the fuel cell operation will not affect the output of the simulation result compared with the high value of lost loads.

Figure 8 shows the dynamics of the fuel tank of the MBS units. From Fig. 8, whenever the fuel volume has been reduced, the MBS unit travels in the system. On the other hand, when

the volume of hydrogen in the fuel tank has been increased or remained constant, the MBS unit is motionless in one of the real stations. To accomplish the load restoration task without interdiction, the lower level of the fuel tank capacity and the final status of the fuel tank have not been restricted. The continuous injection and deployment of hydrogen fuel in the tanks confirms that the proposed method has been successfully applied to the load restoration model, especially under the risk-averse strategy. From the total consumed fuel by the MBS units, the overall distance traveled by each MBS unit can be estimated. The fuel consumption for the congested roads is considered 50% higher than that for the normal traffic roads. The presence of hydrogen storage in the microgrids provides flexibility to refuel the MBS units to accomplish the load restoration task. The involvement of the fuel tank model makes it practical to find the best routing for the MBS units with the least traffic conditions and lower fuel consumption. To chase the MBS units and reveal their role in the load restoration plans, Fig. 9 represents the trajectory of the MBS units under risk-neutral and risk-averse strategies. To verify the effectiveness of the proposed scheduling problem, the routing plans are presented for scenario 12 whereas roads 1-4 and 3-6 are congested between 8:00 to 13:00 and 18:00 to 20:00. For instance, the MBS unit #1 and #3 get stuck in traffic at hours 8:00 and 9:00 under the risk-neutral strategy. Similarly, MBS unit #1 gets stuck in traffic at hours 19:00 and 20:00 when traveling in path $4 \leftrightarrow 1$. The traffic flow influences the fuel consumption and neglecting this fact leads to a defective load restoration mission. The results provided in in Fig. 9 are consistent with the fuel consumption results in Fig. 8. An important point in Fig. 9 was revealed when we compared the risk-neutral and risk-averse strategies. Under the risk-averse strategy, only MBS unit #2 is stuck in the traffic at hours 10:00 and 11:00 and the load restoration trajectory has been determined conservatively and firmly. The MBS units have a key role in serving the critical loads during the power outage. The movability helps the system operator to serve the loads based on priority. In other words, stationary battery storage increases the resiliency of a particular microgrid by supporting the critical and non-critical loads simultaneously. Whereas, the MBS units increase the efficiency and make it available to serve the critical loads instead of non-critical ones during the outages. Figure 10 shows the energy capacity of the MBS units. It is clear that before the fault (before hour 10:00), the MBS units are charged progressively. The charging and discharging status of the MBS units is completely different under the risk-neutral and risk-averse cases due to a different routing plan and renewable outputs. Although the general trend for the MBS units is to operate in discharging mode during the outage time, the MBS units are charged at hours 11:00 and 12:00 under a risk-neutral strategy emphasizing the fact that MBS units can act as critical loads in microgrids and carry the required energy to the neighboring microgrid. Comparing Fig. 10 and Table 6 confirms the validity of the routing and energy management models. The MBS units can charge and discharge electric power only if they are attached to a real station. The state-of-charge in Fig. 10 reveals the key role of the MBS units in load restoration plans as the batteries are discharged during peak times. After hour 17:00 (when the fault is cleared) the state-of-charge of the batteries remained unchanged since the multi-microgrids are connected to the main grid.

C. Resiliency improvement analysis

In order to assess the resiliency enhancement using the proposed method, the resiliency trapezoid for the system is drawn in

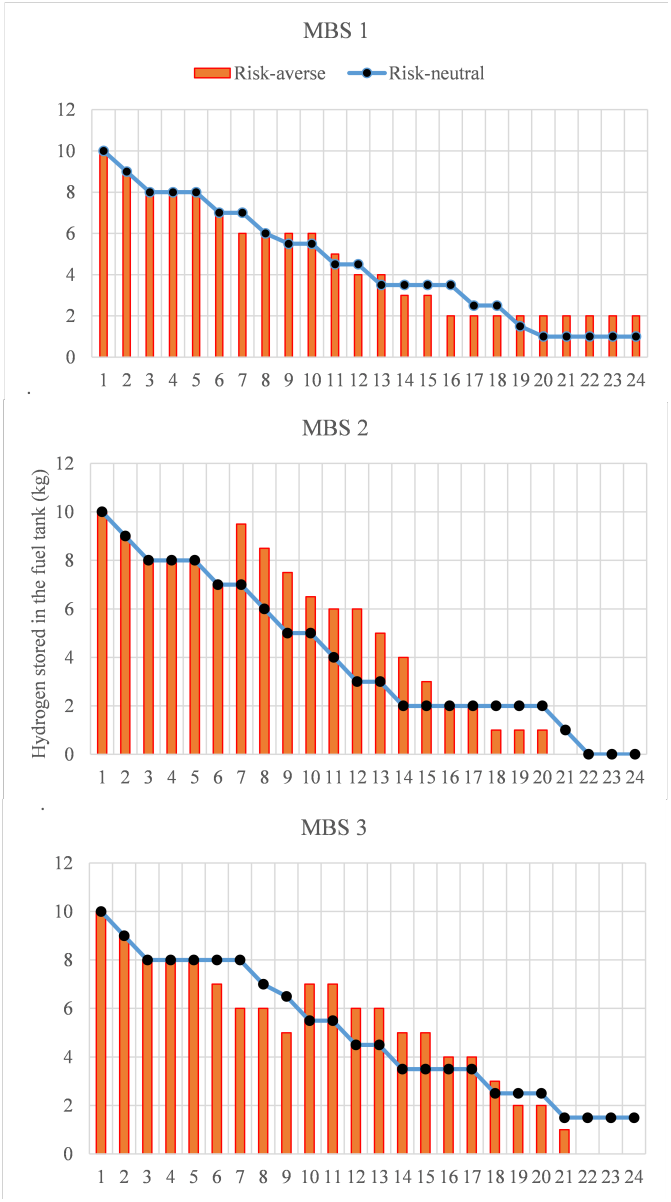

Fig. 8. The realized state of fuel in the tank of MBS units

Risk-neutral	Hour																							
MBS No.	1	2	3	4	5	6	7	8	9	10	11	12	13	14	15	16	17	18	19	20	21	22	23	24
1	1	1↔2	2↔3	3	3	3↔6	6	6↔3	6↔3	3	3↔2	2	2↔1	1	1	1	1↔4	4	4↔1	4↔1	1	1	1	1
2	1	1↔4	4↔5	5	5	5↔6	6	6↔5	5↔4	4	4↔5	5↔6	6	6↔3	3	3	3	3	3	3	3↔2	2↔1	1	1
3	1	1↔2	2↔3	3	3	3	3	3↔6	3↔6	6↔5	5	5↔4	4	4↔5	5	5	5	5↔4	4	4	4↔1	1	1	1
Risk-averse																								
MBS No.	1	2	3	4	5	6	7	8	9	10	11	12	13	14	15	16	17	18	19	20	21	22	23	24
1	1	1↔4	4↔5	5	5	5↔6	6↔3	3	3	3	3↔2	2↔1	1	1↔2	2	2↔1	1	1	1	1	1	1	1	1
2	1	1↔4	4↔5	5	5	5↔4	4	4↔5	5↔6	6↔3	6↔3	3	3↔2	2↔1	1↔4	4↔5	5	5↔4	4	4	4↔1	1	1	1
3	1	1↔4	4↔5	5	5	5↔4	4↔1	1	1↔2	2	2	2↔1	1	1↔2	2	2↔1	1	1↔2	2↔3	3	3↔2	2↔1	1	1

Fig. 9. The routing plan of the MBS units

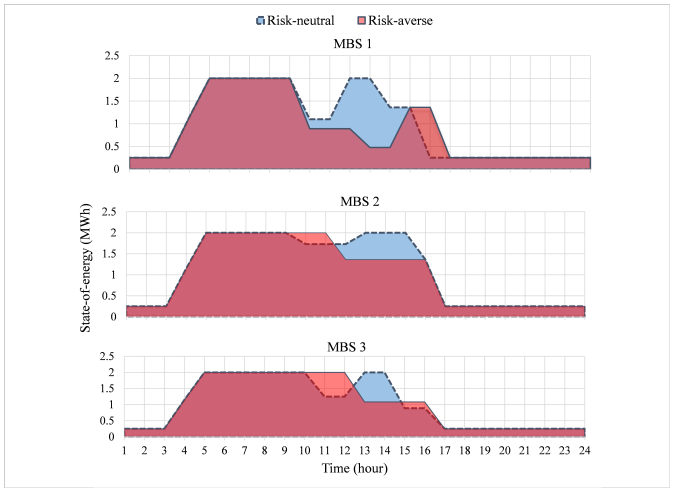

Fig. 10. The realized state of energy of the MBS unit

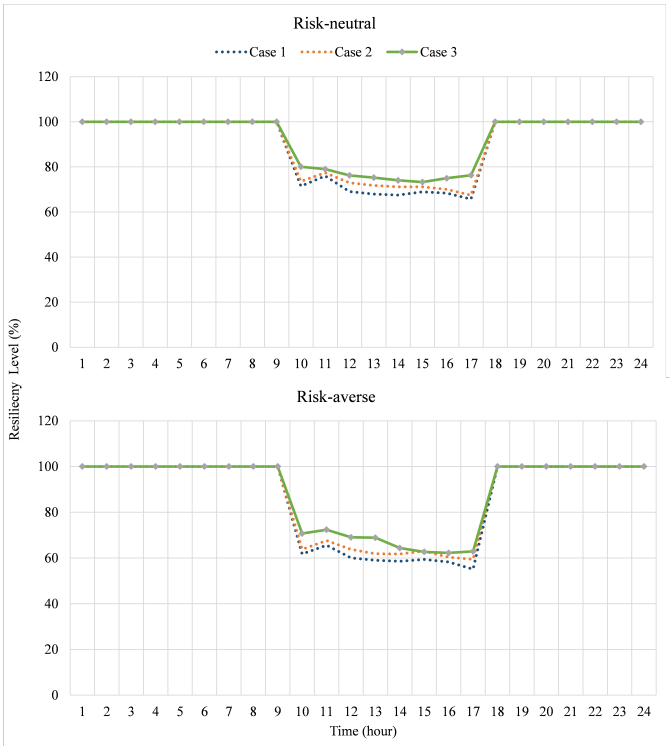

Fig. 11. Comparison between resiliency trapezoids

Fig. 11 for both risk-neutral and risk-averse strategies. The resiliency level is defined as the portion of the total restored critical load versus the total critical load per hour. For three cases, the resiliency trapezoids are drawn. Case 1 is dedicated to a system without hydrogen and MBS units, case 2 is dedicated to a system with hydrogen system and without MBS units, and case 3 is dedicated to a system with full deployment of hydrogen and MBS units. The area under the curves is an index to identify the resiliency improvement. A more unified area under the curve shows a more resilient operation. Obviously, the case without the hydrogen infrastructure and MBS units has the least restored critical load and shows higher fragility under both risk-neutral and risk-averse strategies. The shape of the trapezoid is changed due to hourly changes in the demand level. The integration of the hydrogen system improves the resiliency according to Table 6 in case 2, however, the overall trend is the same. In case 3, the MBS unit not only improves the resiliency level but also changes the shape of the trapezoid affecting the area below the shape. This fact is distinct in the risk-neutral case, in particular. Table 6 summarizes different resiliency assessment indexes. The area below the curve is a general index that includes various information regarding the resiliency of the system, including the ramp of resiliency fall, load disconnection duration, response of corrective strategy, and total load disruption value. From Table 6, case 3 with the optimal coordination of the power and hydrogen resources and MBS dispatch, has the highest resiliency level. The area below the curve in this case covers 92% and 89% of the whole district in risk-neutral and risk-averse cases, respectively. The L-index shows the total curtailed load during the power outage. From Table 7, the total critical load shedding without supportive infrastructure and corrective strategy goes up to 38.65 MW in the risk-neutral strategy and 50.78 MW in the risk-averse strategy. However, the corrective strategies in cases 2 and 3 reduced the total not-supplied critical loads by about 8.3% and 22.2%, respectively in the risk-neutral case. For the risk-averse strategy, the total not-supplied load has been reduced by 7.5% and 16.9%, respectively in cases 2 and 3. The third index in Table 6 shows the fragility of the system, whereas the higher value of case 1 under both risk-neutral and risk-averse cases confirms that the system resiliency has decreased sharply compared with cases 2 and 3. Taking case 1 as a base case, the R-index has been improved by 7% and 8.6% in cases 2 and 3, respectively, for the risk-neutral strategy and by 5.5% and 23.29% for the risk-averse strategy. This fact shows that the corrective strategies remarkably reduced the fragility of the integrated energy system under the risk-averse strategy. The time of power outage for the rest of the non-restored critical loads remains unchanged. In this regard, the T-index shows the total disruption time that shows the critical loads have at least experienced 8-hour outages regardless of the corrective strategies. The reason behind this phenomenon is the generation capacity that is proportioned with the load consumption. The resiliency assessment for the non-critical loads does not show a remarkable achievement for cases 2 and 3 since the majority of the emergency resources are deployed to recover the critical loads. Finally, it should be noted that the MBS units besides the hydrogen infrastructures cannot act as generative resources, and their effectiveness is directly associated with their rated capacity.

D. Discussion

Hydrogen technology has been extensively used in recent decades to increase sustainability and efficiency. According to a report by IEA [32], the hydrogen production cost is anticipated to be $ 0.5-8 per kilogram. For resiliency-oriented programming, the value of lost load in Table 3 has a greater impact on the curtailed load, and by determining a conservative penalty cost (Voll), the hydrogen production cost can be covered. Moreover, the main part of fuel cell operation cost is related to the hydrogen procuration and hydrogen cylinders. In the studied case, the hydrogen production through renewable energies in the microgrids effectively reduces the operational cost of the fuel cell system. In the objective function, the cost of purchasing power from the utility is time dependent that affects the traded power scheme, however, the hydrogen production cost is constant in the daily operation which means it can be ignored for resiliency-

Table 6. Detailed analysis of resiliency for three cases with hydrogen facility

Risk attitude	Case	The unified area below the curve	Total critical load curtailment	The ramp of first resiliency fall	Total load disconnection time
Risk-neutral	1	0.9	38.65 MW	0.285	8 hours
	2	0.91	35.44 MW	0.264	8 hours
	3	0.92	30.08 MW	0.199	8 hours
Risk-averse	1	0.87	50.78 MW	0.382	8 hours
	2	0.88	46.98 MW	0.361	8 hours
	3	0.89	42.17 MW	0.293	8 hours

Table 7. Analysis of resiliency for case 3 with stationary battery storage facility

Risk attitude	Case	Total critical load curtailment
Risk-neutral	With hydrogen storage	30.08 MW
	With stationary battery storage	30.37 MW
Risk-averse	With hydrogen storage	42.17 MW
	With stationary battery storage	43.38 MW

oriented operation. As an alternative, the hydrogen storage facilities in microgrids 2 and 4 can be replaced with equivalent electric battery storage systems. To this end, two battery storage systems with a maximum capacity of 4 MWh/4 MW with charging/discharging efficiency of 95% are considered in the corresponding microgrids. It should be noted that hydrogen production through a water electrolyzer is available to refuel the MBS units. Table 7 represents the total critical load curtailment (L-index) for both risk-neutral and risk-averse strategies in the presence of stationary battery storage systems. The results in Table 7 confirm that the presence of hydrogen storage is promoted. Furthermore, the following issues justifies the use of hydrogen storage facility.

1. The critical load curtailment is lesser with the hydrogen facility under both risk attitudes. The analysis revealed that the presence of hydrogen storage makes it possible to refuel the MBS units more actively that reduces the total load curtailment.
2. The electricity produced by the fuel cell device with hydrogen storage is renewable and green and does not contribute to environmental pollution despite the battery storage systems with toxic effects.
3. Batteries need frequent charging/discharging, while the fuel cell beside the hydrogen storage provides a longer power generation capacity. Moreover, the stored hydrogen can be sold in the industry park as a parallel economic project.

4. CONCLUSION

This paper proposed a hybrid stochastic-robust approach for resilient scheduling of renewable-dominant integrated power and hydrogen microgrids to enhance the electric load recovery after a grid outage. By using the proposed approach, the system operator can take into account several serious uncertainties and make decisions based on risk acceptance. The uncertainty of the traffic flow affects the arrival time of the MBS units and the overall fuel consumption which was modeled by stochastic programming and the uncertainty of the renewables that challenges the overall scheduling and the load restoration plans was handled by the robust optimization. The simulation has been carried out on a 6-microgrid test system in three cases, in which the grid outage is considered an emergency condition with a total duration of 8 hours. The results confirmed the effective cooperation of the power and hydrogen carriers to provide the hydrogen fuel of the MBS units and generate a short-term energy storage capacity. From the results, the critical load curtailment without supportive strategies is 38.65 MW and 50.78 MW for risk-neutral and risk-averse strategies. By using the proposed resiliency-oriented strategy, the area below the resiliency trapezoid covered 92% and 89% of the whole district in risk-neutral and risk-averse cases, respectively. In more detail, the proposed method can survive 22.17% and 16.95% of critical loads with risk-neutral and risk-averse perspectives, respectively. Moreover, the fragility index that shows the ramp of resiliency fall has been improved by 30% and 23%, respectively, under risk-neutral and risk-averse cases. The proposed methodology could not improve the interruption time due to the limited capacity of the recovery strategy and the duration of load curtailment remained at 8 hours in all cases. In the end, the performance of stationary battery storage and hydrogen storage was compared. The analysis revealed that the recovered load using stationary battery storage is considerable but the presence of hydrogen storage can help the MBS refueling process and optimize the load recovery objective.

REFERENCES

1. Bintoudi AD, Demoulias C. Optimal isolated microgrid topology design for resilient applications. Applied Energy 2023;338:120909.

2. Abdelsalam HA, Eldosouky A, Srivastava AK. Enhancing distribution system resiliency with microgrids formation using weighted average consensus. International Journal of Electrical Power & Energy Systems 2022;141:108161.

3. Zadsar M, Ansari M, Ameli A, Abazari A, Ghafouri M. A two-stage framework for coordination of preventive and corrective resiliency enhancement strategies in power and

gas distribution systems. International Journal of Electrical Power & Energy Systems 2023;148:108914.

4. Malek AF, Mokhlis H, Muhammad MA, Bajwa AA, Mansor NN, Jamian JJ. Resilience based decision metrics for dispatching mobile emergency truck generators in distribution system. 2021 IEEE International Conference in Power Engineering Application (ICPEA), IEEE; 2021, p. 233–8.

5. Mayyas A, Wei M, Levis G. Hydrogen as a long-term, large-scale energy storage solution when coupled with renewable energy sources or grids with dynamic electricity pricing schemes. International Journal of Hydrogen Energy 2020;45:16311–25. https://doi.org/https://doi.org/10.1016/j.ijhydene.2020.04.163.

6. Brunaccini G, Sergi F, Aloisio D, Randazzo N, Ferraro M, Antonucci V. Fuel cells hybrid systems for resilient microgrids. International Journal of Hydrogen Energy 2019;44:21162–73. https://doi.org/https://doi.org/10.1016/j.ijhydene.2019.04.121.

7. Shahbazbegian V, Shafie-khah M, Laaksonen H, Strbac G, Ameli H. Resilience-oriented operation of microgrids in the presence of power-to-hydrogen systems. Applied Energy 2023;348:121429.

8. Liu J, Cao X, Xu Z, Guan X, Dong X, Wang C. Resilient operation of multi-energy industrial park based on integrated hydrogen-electricity-heat microgrids. International Journal of Hydrogen Energy 2021;46:28855–69. https://doi.org/https://doi.org/10.1016/j.ijhydene.2020.11.229.

9. Gharehveran SS, Ghassemzadeh S, Rostami N. Two-stage resilience-constrained planning of coupled multi-energy microgrids in the presence of battery energy storages. Sustainable Cities and Society 2022;83:103952.

10. Saboori H, Jadid S. Mobile and self-powered battery energy storage system in distribution networks–Modeling, operation optimization, and comparison with stationary counterpart. Journal of Energy Storage 2021;42:103068.

11. Dugan J, Mohagheghi S, Kroposki B. Application of mobile energy storage for enhancing power grid resilience: A review. Energies 2021;14:6476.

12. Abdeltawab H, Mohamed YA-RI. Mobile Energy Storage Sizing and Allocation for Multi-Services in Power Distribution Systems. IEEE Access 2019;7:176613–23. https://doi.org/10.1109/ACCESS.2019.2957243.

13. Chen Y, Zheng Y, Luo F, Wen J, Xu Z. Reliability evaluation of distribution systems with mobile energy storage systems. IET Renewable Power Generation 2016;10:1562–9.

14. Kim J, Dvorkin Y. Enhancing Distribution System Resilience With Mobile Energy Storage and Microgrids. IEEE Transactions on Smart Grid 2018. https://doi.org/10.1109/TSG.2018.2872521.

15. Sadegh AR, Nazar MS, Shafie-khah M, Catalao JPS. Optimal resilient allocation of mobile energy storages considering coordinated microgrids biddings. Applied Energy 2022;328:120117.

16. Lee J, Razeghi G, Samuelsen S. Utilization of Battery Electric Buses for the Resiliency of Islanded Microgrids. Applied Energy 2023;347:121295.

17. Wang J, Li Y, Bian J, Yu Z, Zhang M, Wang C, et al. Multi-stage resilient operation strategy of urban electric–gas system against rainstorms. Applied Energy 2023;348:121507.

18. Bose S, Chowdhury S, Zhang Y. Co-optimization of Battery Routing and Load Restoration for Microgrids with Mobile Energy Storage Systems. 2022 IEEE Power & Energy Society General Meeting (PESGM), IEEE; 2022, p. 1–5.

19. Nazemi M, Dehghanian P, Lu X, Chen C. Uncertainty-Aware Deployment of Mobile Energy Storage Systems for Distribution Grid Resilience. IEEE Transactions on Smart Grid 2021. https://doi.org/10.1109/TSG.2021.3064312.

20. Mehrjerdi H, Mahdavi S, Hemmati R. Resilience maximization through mobile battery storage and diesel DG in integrated electrical and heating networks. Energy 2021;237:121195.

21. Rezaee Jordehi A, Mansouri SA, Tostado-Véliz M, Iqbal A, Marzband M, Jurado F. Industrial energy hubs with electric, thermal and hydrogen demands for resilience enhancement of mobile storage-integrated power systems. International Journal of Hydrogen Energy 2024;50:77–91. https://doi.org/https://doi.org/10.1016/j.ijhydene.2023.07.205.

22. Zhou Z, Zhang X, Guo Q, Sun H. Analyzing power and dynamic traffic flows in coupled power and transportation networks. Renewable and Sustainable Energy Reviews 2021;135:110083.

23. Yao S, Wang P, Liu X, Zhang H, Zhao T. Rolling optimization of mobile energy storage fleets for resilient service restoration. IEEE Transactions on Smart Grid 2019;11:1030–43.

24. Xu Y, Wang Y, He J, Su M, Ni P. Resilience-oriented distribution system restoration considering mobile emergency resource dispatch in transportation system. IEEE Access 2019;7:73899–912.

25. Erenoğlu AK, Erdinç O. Post-Event restoration strategy for coupled distribution-transportation system utilizing spatiotemporal flexibility of mobile emergency generator and mobile energy storage system. Electric Power Systems Research 2021;199:107432.

26. Saboori H, Mehrjerdi H, Jadid S. Mobile battery storage modeling and normal-emergency operation in coupled distribution-transportation networks. IEEE Transactions on Sustainable Energy 2022;13:2226–38.

27. Akbari-Dibavar A, Mohammadi-Ivatloo B, Zare K, Anvari-Moghaddam A. Optimal Scheduling of a Self-Healing Building Using Hybrid Stochastic-Robust Optimization Approach. IEEE Transactions on Industry Applications, 2022. https://doi.org/10.1109/TIA.2022.3155585.

28. Mehrjerdi H. Off-grid solar powered charging station for electric and hydrogen vehicles including fuel cell and hydrogen storage. International Journal of Hydrogen Energy 2019. https://doi.org/10.1016/j.ijhydene.2019.03.158.

29. Bertsimas D, Sim M. Robust discrete optimization and network flows. Mathematical Programming, vol. 98, 2003, p. 49–71. https://doi.org/10.1007/s10107-003-0396-4.

30. Wang Z, Chen B, Wang J, Chen C. Networked microgrids for self-healing power systems. IEEE Transactions on Smart Grid 2015;7:310–9.

31. Cplex G. The solver manuals. Gams/Cplex, 2014 n.d.

32. Global Hydrogen Review 2021 n.d. https://www.iea.org/reports/global-hydrogen-review-2021/executive-summary.

33. A. Akbari-Dibavar, V. Sohrabi Tabar, S. Ghassem Zadeh, and R. Nourollahi, "Two-stage robust energy management of a hybrid charging station integrated with the photovoltaic system," International Journal of Hydrogen Energy, vol. 46, no. 24, pp. 12701–12714, 2021, doi: https://doi.org/10.1016/j.ijhydene.2021.01.127.